Flat-field families / Wheel jitter

Pascal GALLAIS - SAp/DAPNIA/CEA Saclay

Extracted from the document available at:

isowww.estec.esa.nl/users/expl_lib/CAM/report_trend_5.ps.gz

Report on the trend analysis of the CAM daily Calibration measurements

Version 1.0

P. Gallais, O. Boulade
Service d'Astrophysique, DAPNIA, CEA/Saclay
91 191 Gif-sur-Yvette cedex, France
September 19, 1998

1 Purpose of the document **2**

2 Data acquisition and data reduction **3**
2.1 The sequences of measurements . . . 3
2.1.1 The de-activation sequence . . . 3
2.1.2 The hand-over sequence . . . 5
2.1.3 Statistics on the whole sample . . . 5
2.2 Data reduction . . . 5
2.2.1 Dark current measurements . . . 5
2.2.2 Flat-Field measurements . . . 6

3 General trends of basic parameters **7**
3.1 SW channel . . . 7
3.1.1 Dark current measurements . . . 7
3.1.2 Responsivity . . . 9
3.2 LW channel . . . 9
3.2.1 Dark current measurements . . . 9
3.2.2 Responsivity . . . 10

4 On the use of the daily measurements **14**
4.1 The variations of the dark measurements . . . 15
4.2 Wheel jitter . . . 17
4.3 Saturation effects . . . 23
4.4 Consequences of the revolution 196 problem . . . 25
4.5 About the LW RESET levels . . . 26
4.5.1 General trend . . . 26
4.5.2 Events . . . 26

5 Conclusions **28**

6 References **28**

Annex A: Gallery of LW images **29**

4.2 Wheel jitter

As seen in section 3.1.2, the SW flat-field measurements present a multi-modal distribution both through the SW1 and SW3 filters.

This phenomenon can be explained by a combination of different repositioning uncertainties of some wheels in the gearwheel, following an optical reconfiguration of the camera. It affects both LW and SW measurements.

Assuming that the median flat-field measurement derived from the whole set of measurements is the ideal flat-field, then we can correct each individual image for the pixel-to-pixel response variation. At the end of this operation, the images are not as flat as we could expect. They display a clear circular pattern which can be attributed to a change of the position of the centre of the illumination field in the images.

The multi-modal distribution is well seen in the case of the images obtained during the deactivation flat-field measurement of the SW detector through the SW3 filter (see figure 12, (the signals have been corrected for the general drift of the response).

Because a circular pattern, moving in the horizontal direction of the image (y axis of the spacecraft) is observed, we can consider the left and right parts of the detector for the analysis.

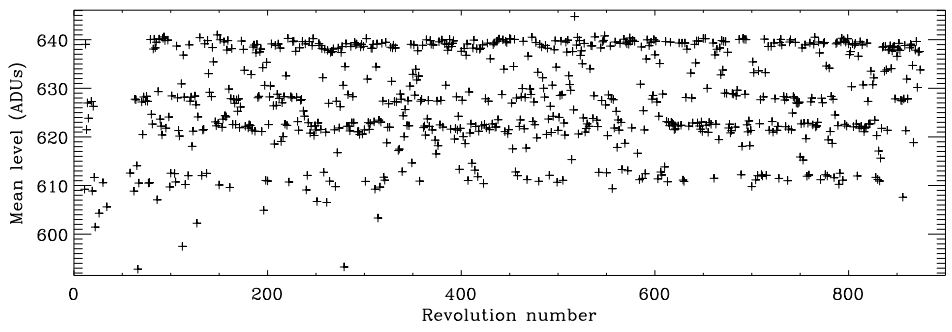

Figure 12: Mean level on SW detector of flat-field measurements through the SW3 filter obtained during de-activation sequence.

In figure 13, we plotted, in the case of the flat-field measurement through SW3 during deactivation, the mean signal over the left part of the detector minus the mean signal over the right part of the detector against the mean signal over the whole array: points are clearly distributed over 8 well defined regions of the plot.

In order to characterize each family of points, and to establish the physical links which can exist between families, we derived, for each set of points, a median image representative of the group. Among the 4 main families identified in figure 12 (named Fam1, Fam2, Fam3 and Fam4) and which clearly appear, 2 of them (Fam2 and Fam4) are split in 3 groups depending on the level of the difference between their right and left parts (Fam2a,b,c and Fam4a,b,c).

The median images for each group are displayed in figure 14, together with the image ratios of linked families. The images of the signal show that the center of illumination is displaced along a sequence depending on the difference left-minus-right. The 2 sequences of evolution are: Fam1, Fam2a, Fam2b and Fam2c for the first sequence and Fam3, Fam4a, Fam4b and Fam4c for the second sequence. Along these sequences, and in similar ways, the center of illumination is moving from the left to the right, i.e along the $-y$ axis of the spacecraft.

For 2 values of the difference left-minus-right, the image ratios show the same pattern in the 2 sequences. A displacement of the center of the illumination field is evident. This displacement being done in the y axis direction, a poor reproducibility of the selection wheel position due to play in the gear, favouring four positions, could explain this result. We notice that even if these privileged positions of the wheel exist, intermediate positions seem to occur, and these invite us to link Fam1 to Fam2 and Fam3 to Fam4.

In another way, each couple of families which have the same difference left-minus-right display the same kind of pattern. For instance, for Fam1 and Fam3, the pattern is vignetted on the right, while for Fam2c and Fam4c, the pattern is vignetted on the left. We can then define 4 couples of families: (Fam1, Fam3), (Fam2a, Fam4a), (Fam2b, Fam4b) and (Fam2c, Fam4c), and the ratios of the images in a each couple are similar for the 4 couples. The similarity indicates that another effect is contributing to the observed multi-modal distribution of SW response throughout the mission. The derived pattern does not allow one to clearly identify the origin of the bimodal distribution. Can this pattern be linked to a displacement of the lens wheel due to play in the gear (because its movement displaces images in the z axis direction) leading to a variation of the illumination field on the detector ? In fact, this last effect is responsible for the quadri-modal distribution initially observed.

Now, we have at our disposal a set of 8 images representative of the combinations of the different basic patterns. These images can be used on the whole set of measurements of the SW responsivity for comparison, associating one of the 8 images with each image obtained during the ISO mission, the criterion of selection being the minimisation of the spatial noise of the image ratio. This has been done and the results are displayed on figure 15. After comparison, the multi-modal distribution of points disappeared and the dispersion has been reduced from 4.1% (global dispersion) to 0.6% (in the central peak, the same as the dispersion measured in each individual peak before correction).

We made the same kind of analysis for the LW flat-field measurements. As for measurements of the SW channel, measurements of the LW channel are also affected by wheel jitter. This effect is seen in figure 16, where we plotted the mean signal over the array against the difference between the mean value on the left part and the mean value on the right part of the detector. The points are more scattered than the SW ones on this kind of graph. Using the same method as used in the SW case, we derived 4 families of points. These images and the ratio between images are displayed in figure 16. The ratio between each family member shows clearly a pattern which corresponds to a move of the center of illumination produced by the poor reproducibility of, in this case, one wheel. Because the move is observed in the y direction, the concerned wheel is certainely the selection wheel.

A poor reproducibility of the selection wheel due to play in the gear has previously been observed in science data, on the edge of the Fabry mirror: in these data, either the first or the last column can be vignetted. A detailed modelling, taking into account the optical gemetry of the camera, could provide an estimation of the effects of the play of the gear on the movement of the pattern in the focal plane.

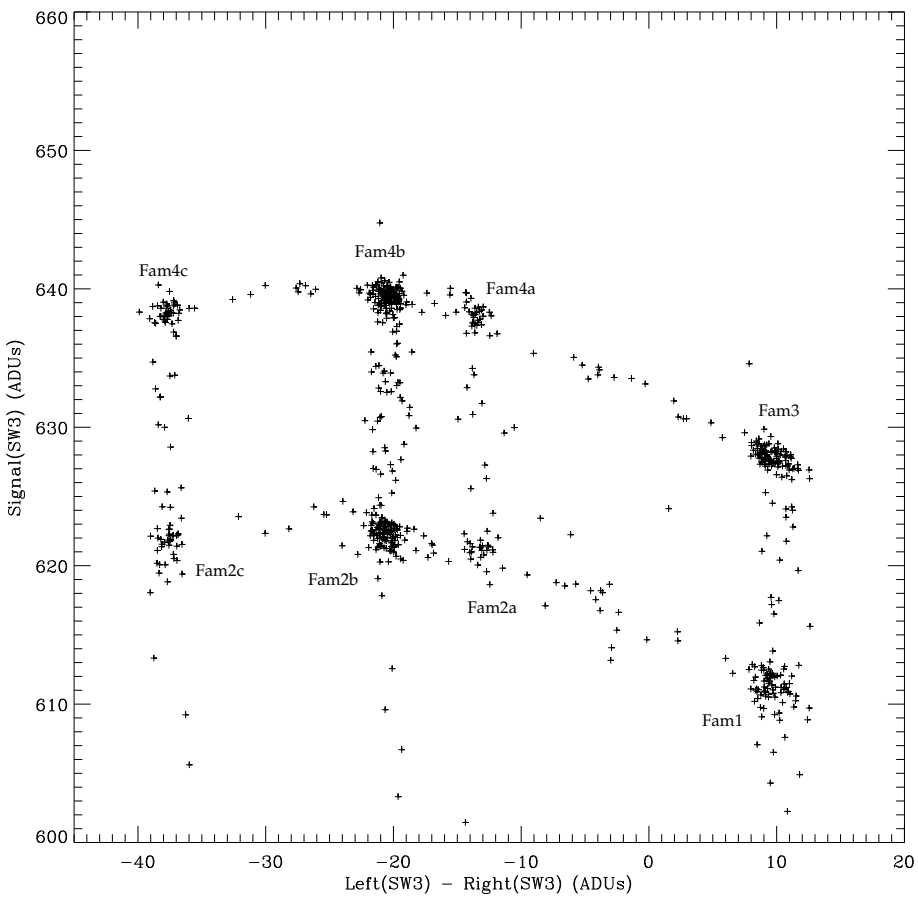

Figure 13: SW deactivation flat-field: Mean value over the SW array versus difference between the left part of the detector and the right part of the detector (y axis of the satellite is oriented from right to left).

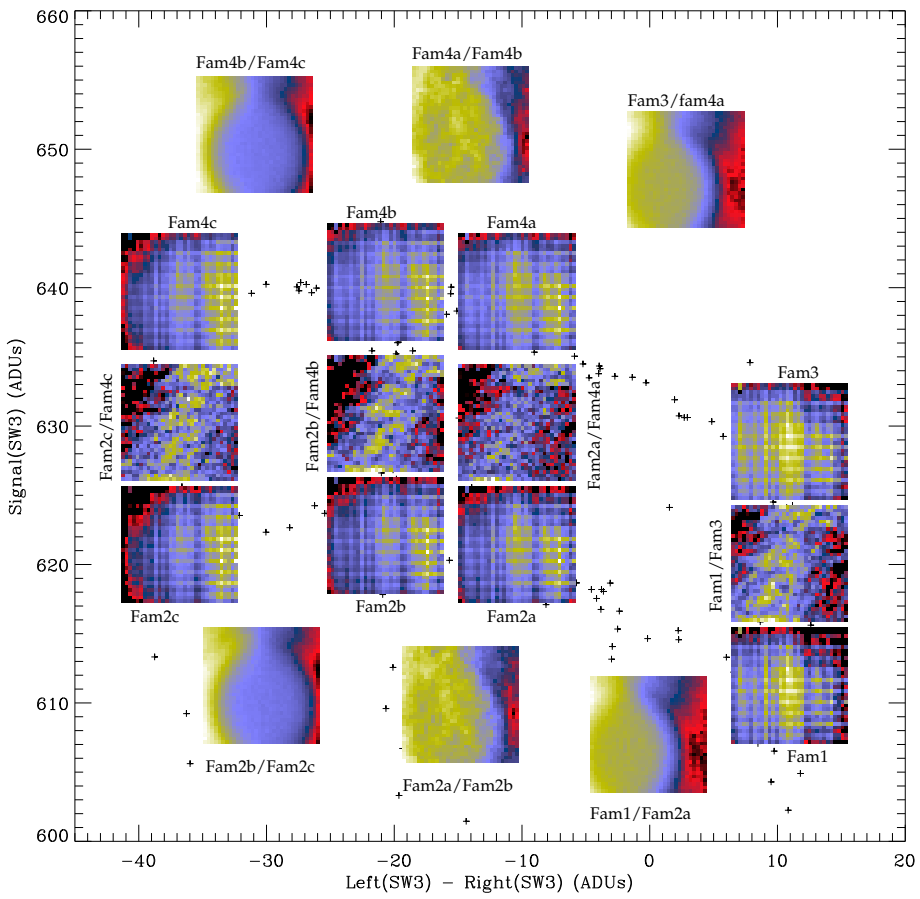

Figure 14: SW deactivation flat-field: same plot as figure 13 in which we superimposed the images of the ICD illumination and the image ratios between couples of families.

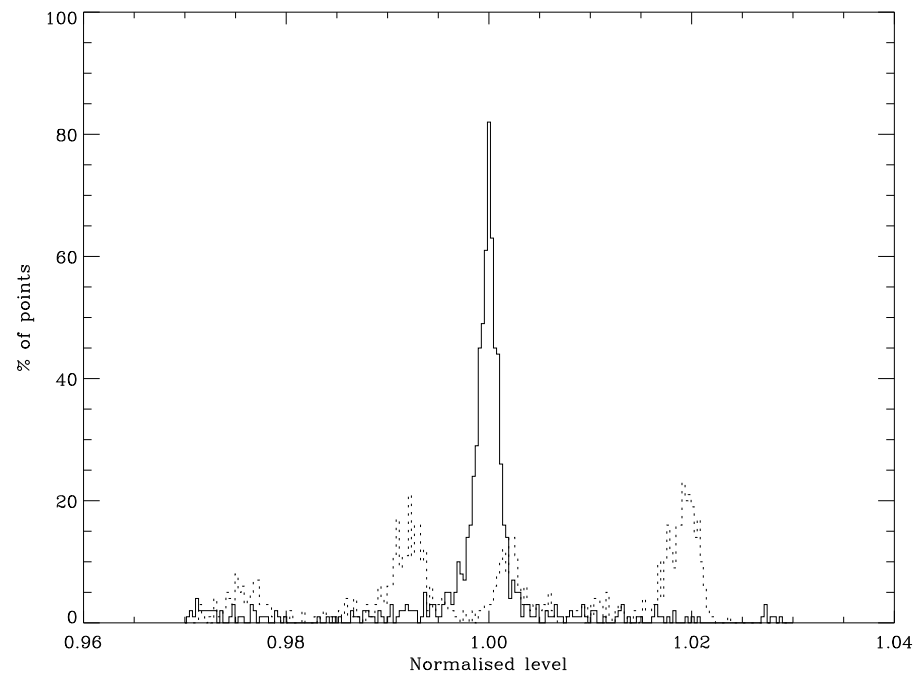

Figure 15: Histogram of the distribution of mean signal of flat-field measurements (corrected for drift) before (dotted line) and after (full line) correction for wheel jitter.

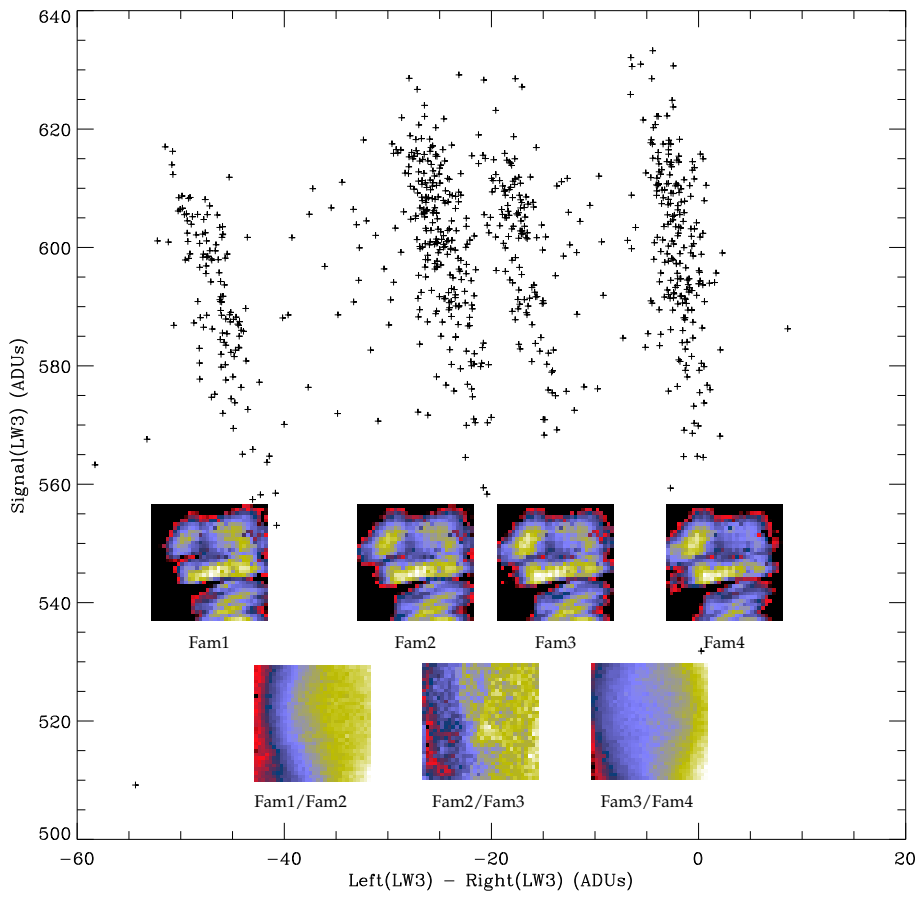

Figure 16: LW deactivation flat-field measurements: Mean value over the LW array against difference between the left part of the detector and the right part of the detector (y axis of the satellite is oriented from left to right). The images of the ICD illumination for each family of points and the image ratios between couples of families are also displayed.

SW3 deactivation flat-field

Raw images

Rev. 500 - 599

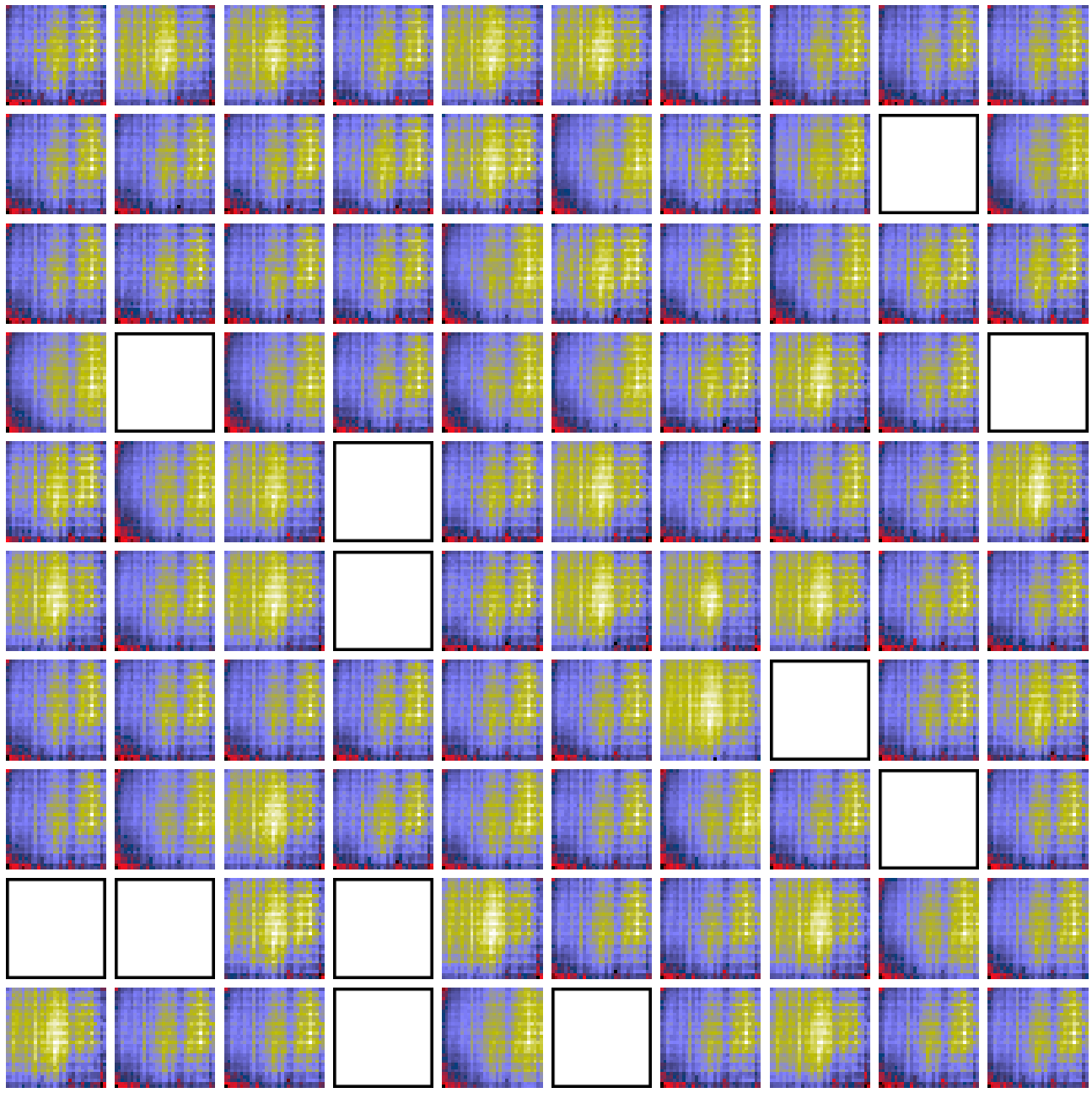

FFSW3_500_599.PS

SW3 deactivation flat-field

Raw values

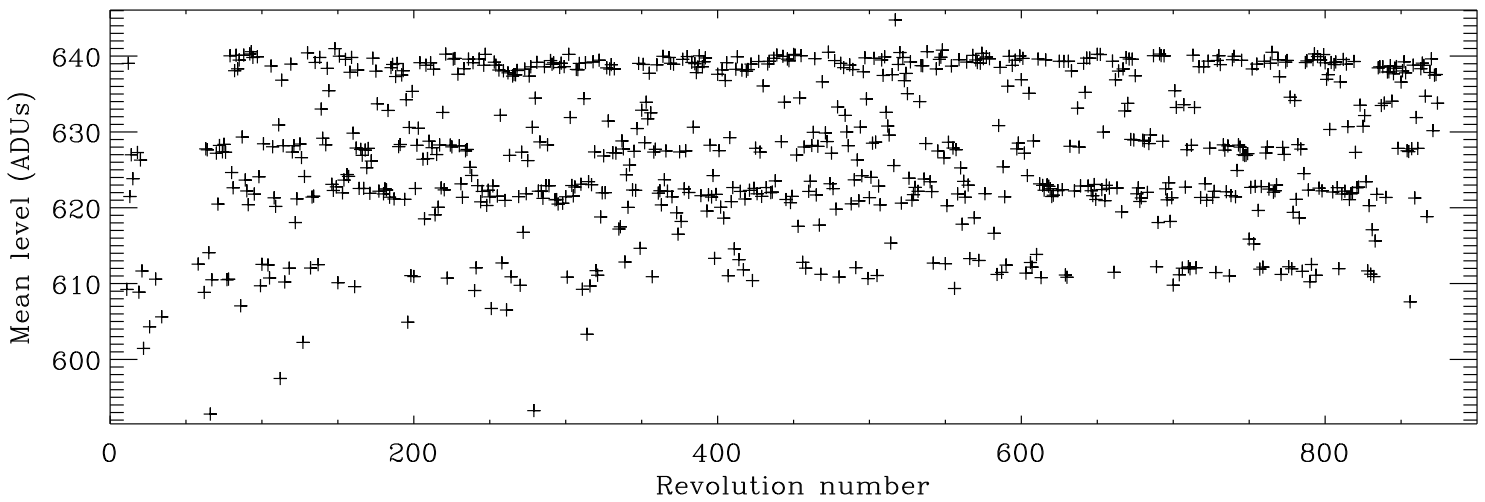

SW3 deactivation flat-field

Uncorrected for wheel jitter

Rev. 100 - 199

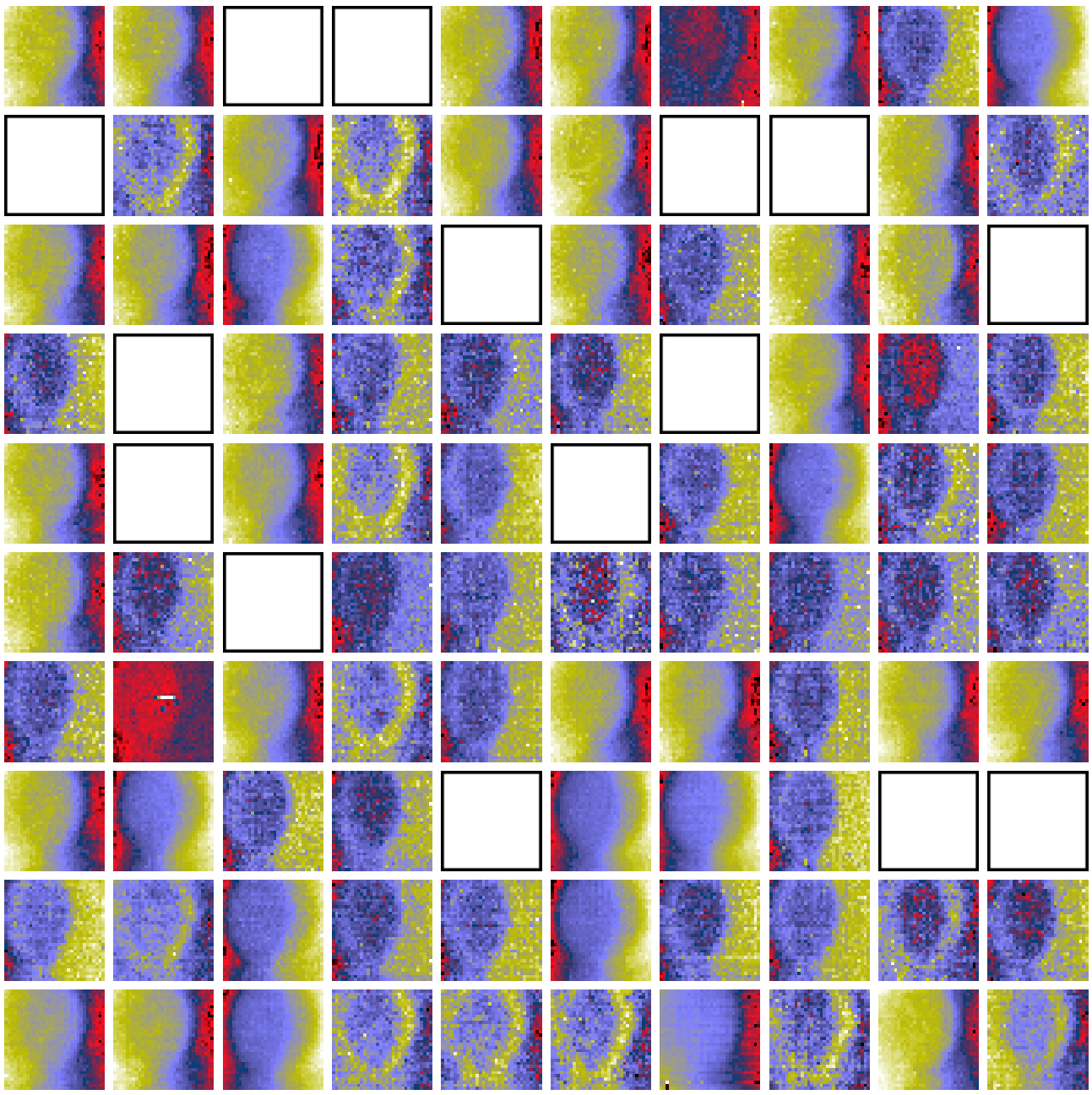

SW3_100_199.PS

SW3 deactivation flat-field

Uncorrected for wheel jitter

Rev. 500 - 599

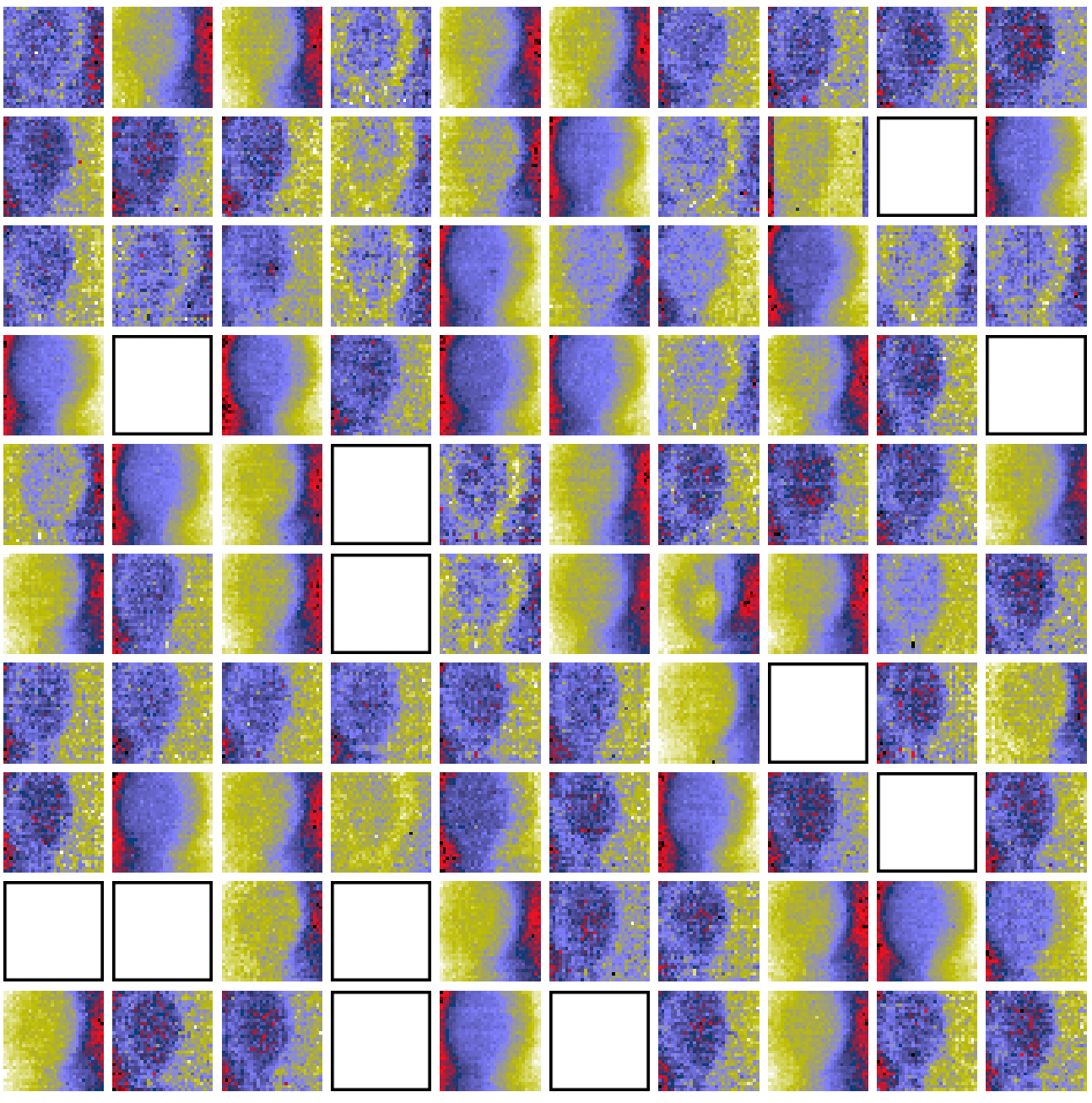

SW3_500_599.PS

SW3 deactivation flat-field

Mean versus (Left - Right)

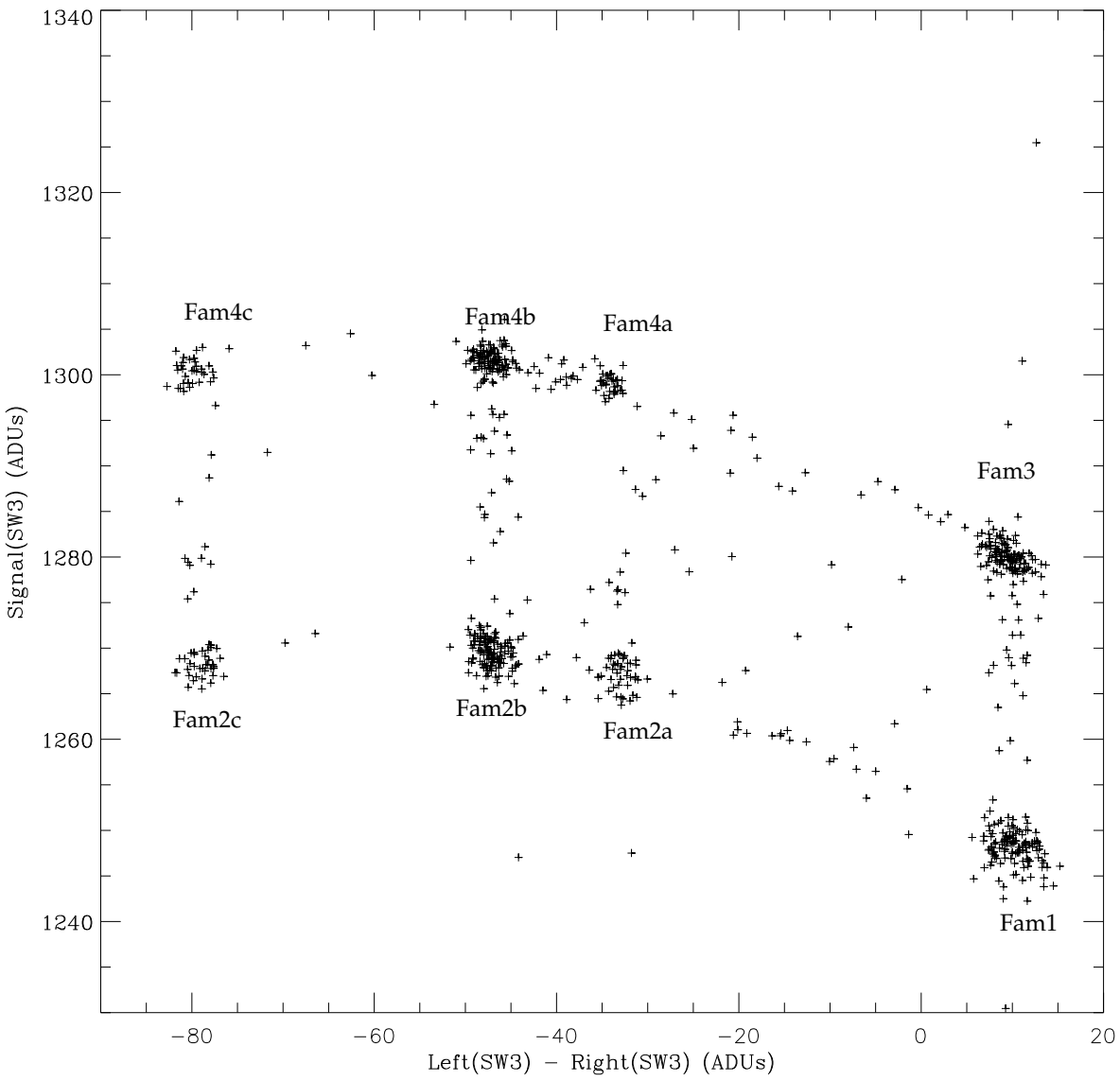

SW3 deactivation flat-field

Mean versus (Left - Right)

Images families

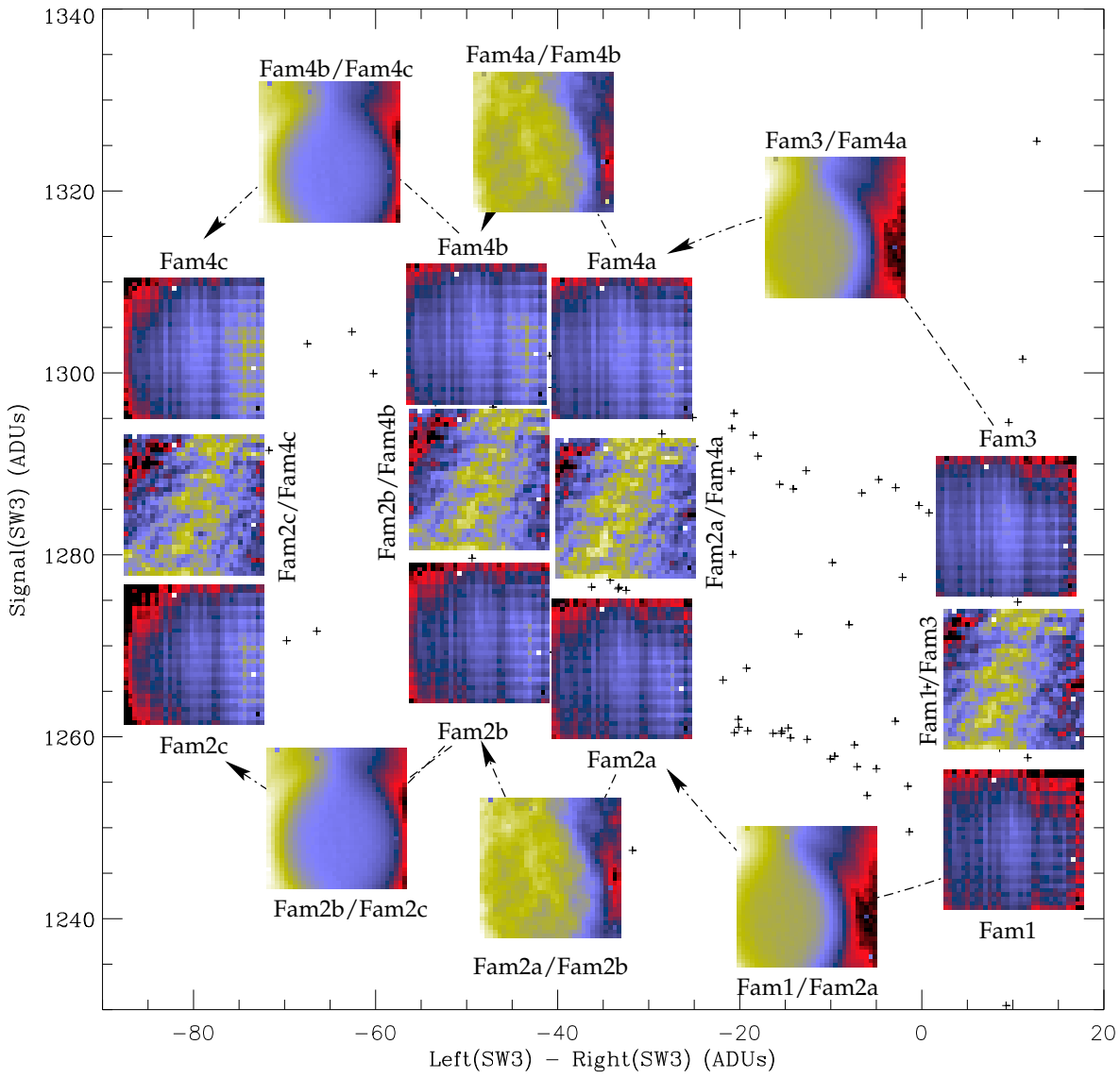

SW3 deactivation flat-field

Corrected values

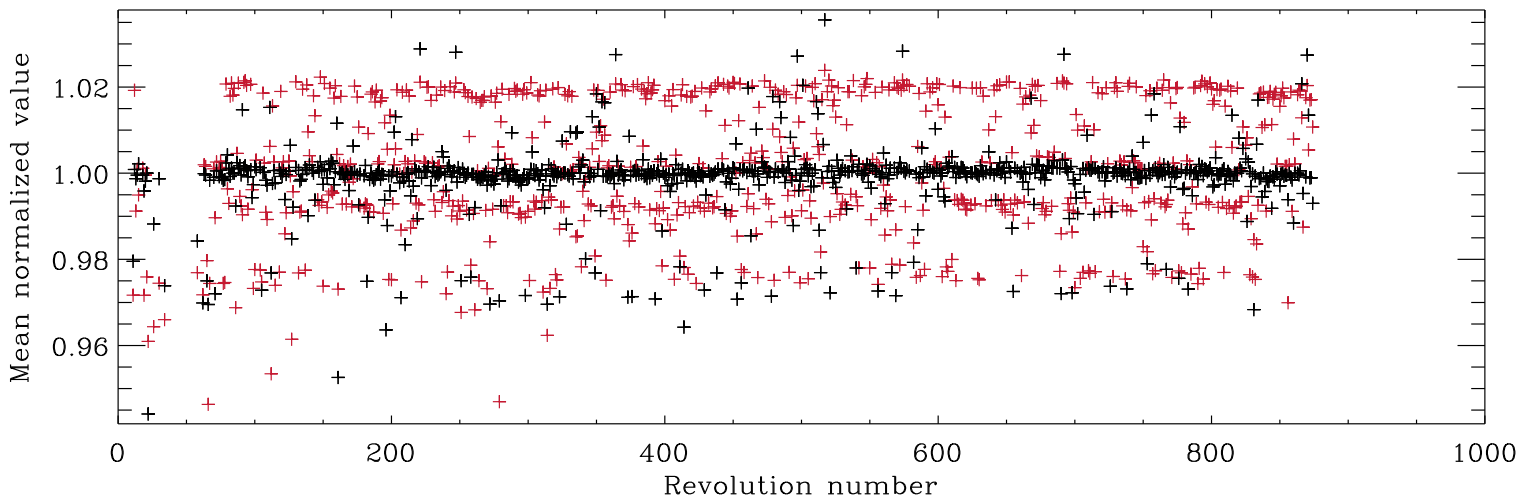

+ Before correction for wheel jitter

+ After correction for wheel jitter

SW3 deactivation flat-field

Distribution of points
for all revolutions

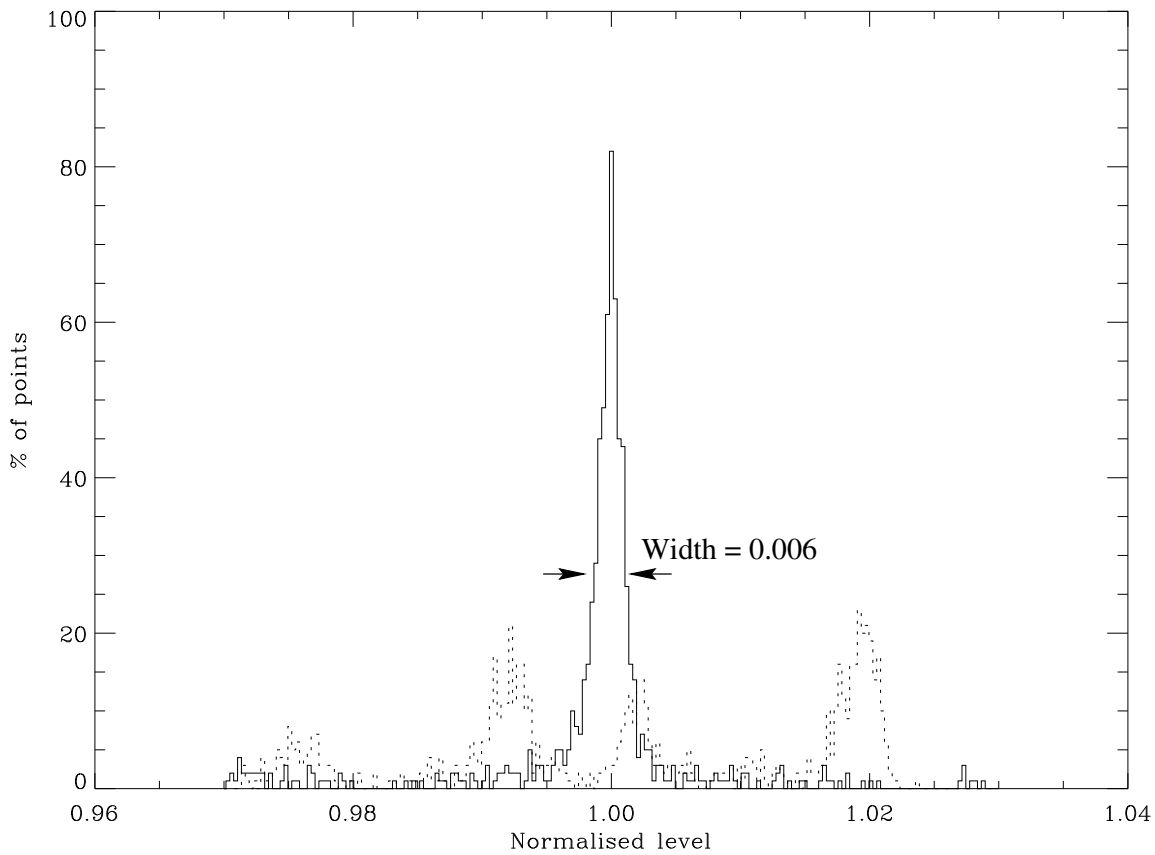

..... Before correction for wheel jitter

——— After correction for wheel jitter

SW3 deactivation flat-field

Corrected for wheel jitter

Rev. 100 - 199

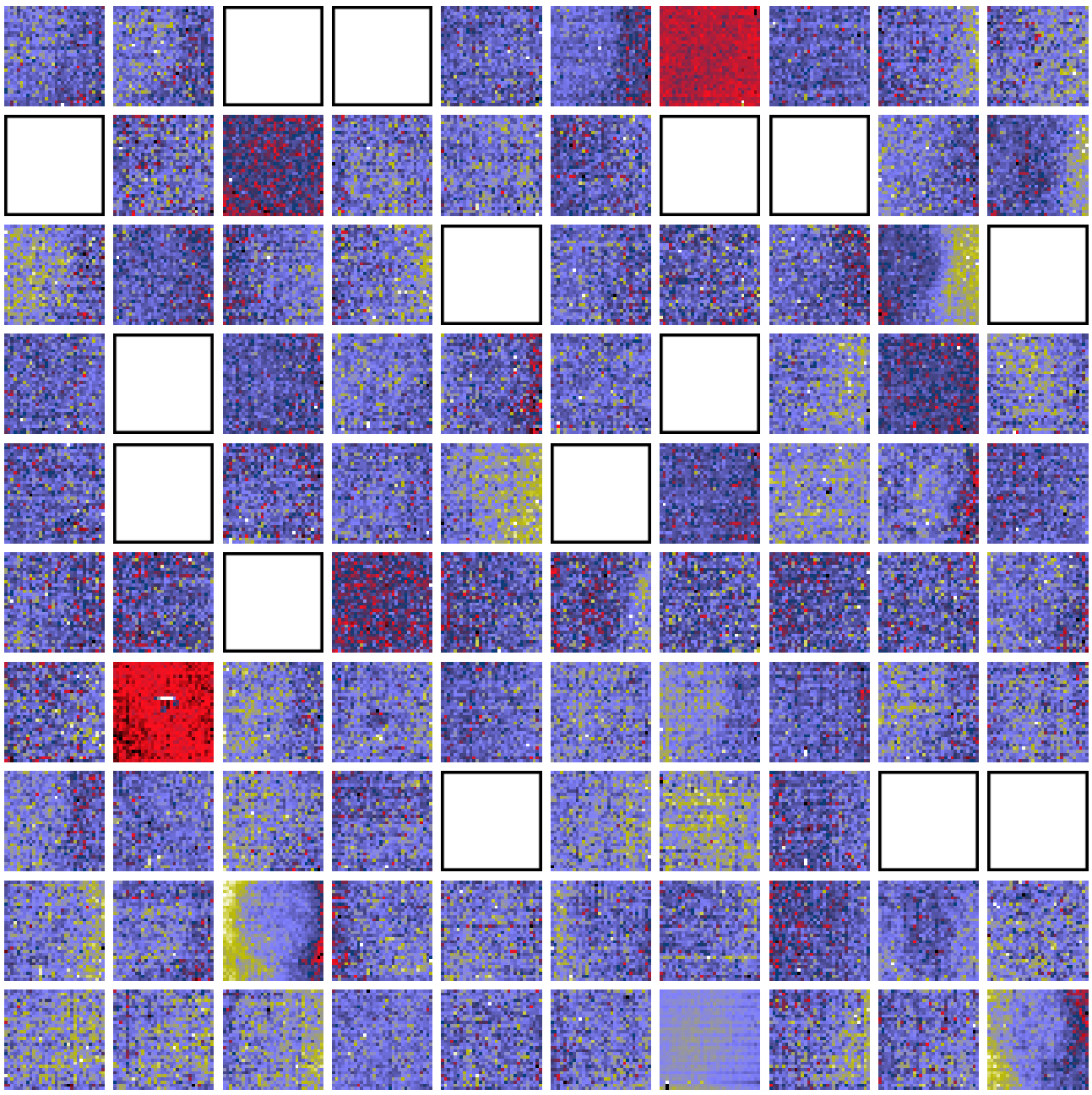

SW3_CORR_100_199.PS

SW3 deactivation flat-field

Corrected for wheel jitter

Rev. 500 - 599

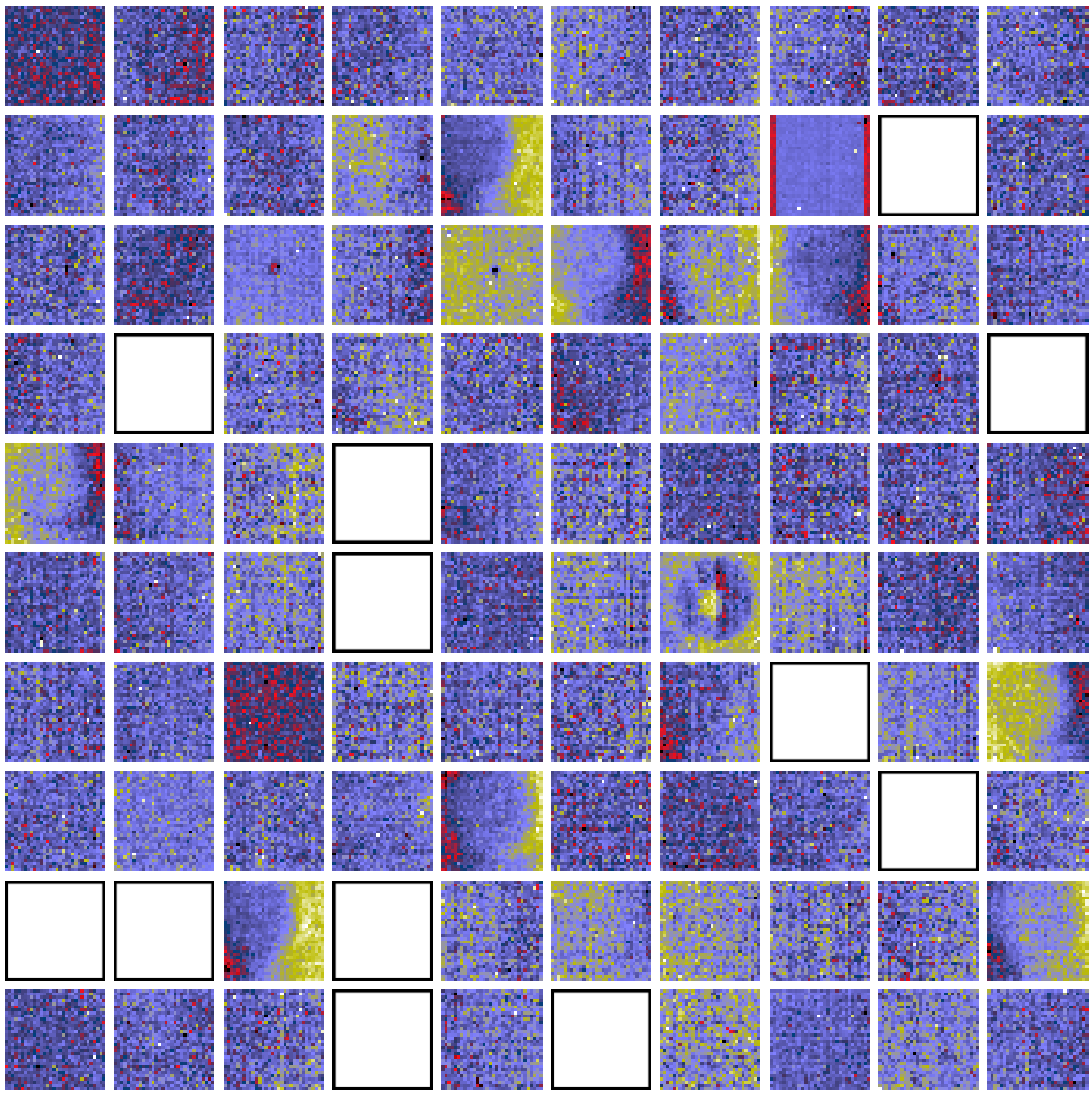

SW3_CORR_500_599.PS

LW3 deactivation flat-field

Raw images

Rev. 200 - 299

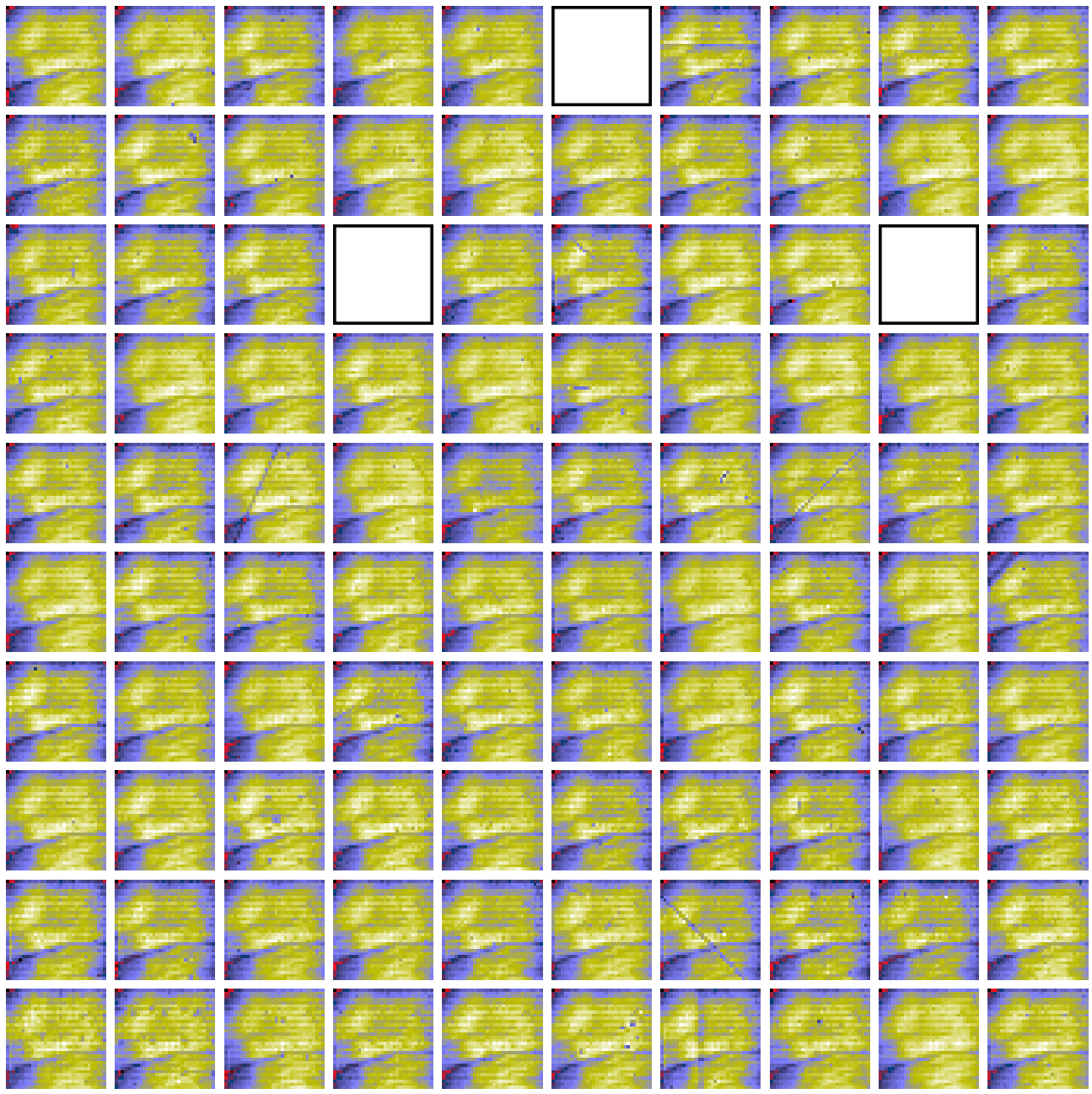

FFLW3_200_299.PS

LW3 deactivation flat-field

Mean versus (Left - Right)

Images families

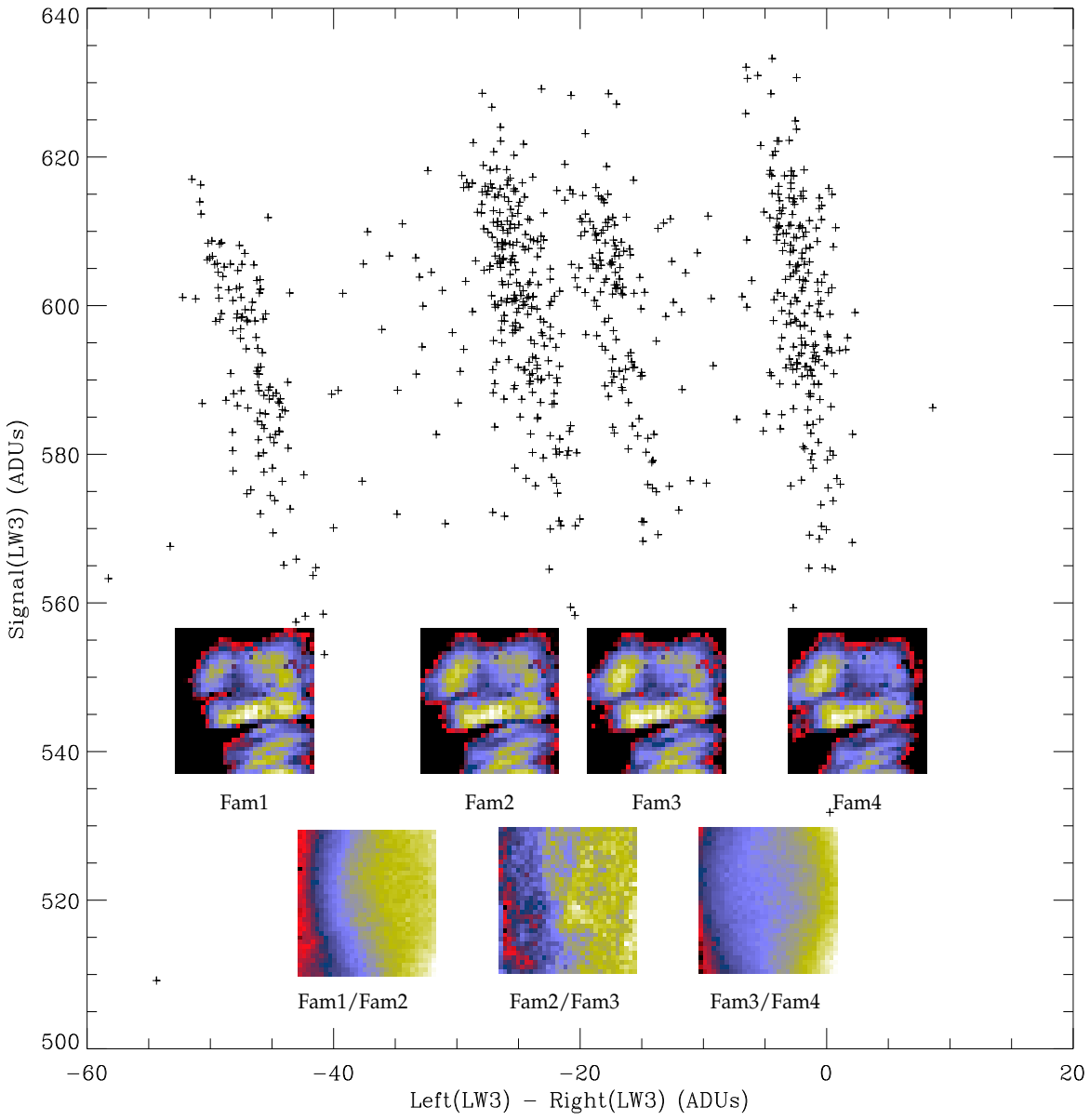

LW3 deactivation flat-field

Uncorrected for wheel jitter

Rev. 200 - 299

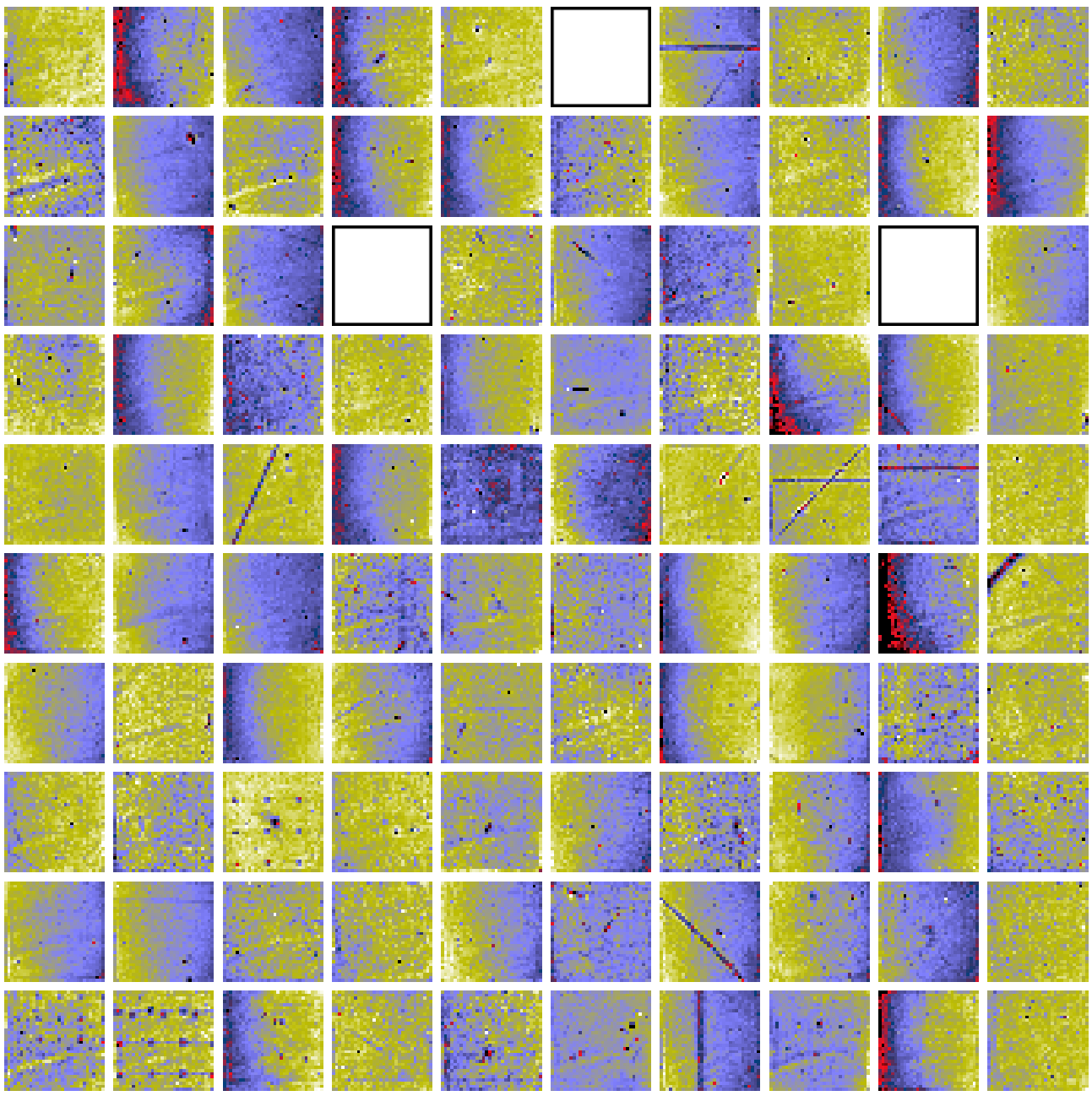

LW3_200_299.PS

LW3 deactivation flat-field

Uncorrected for wheel jitter

Rev. 500 - 599

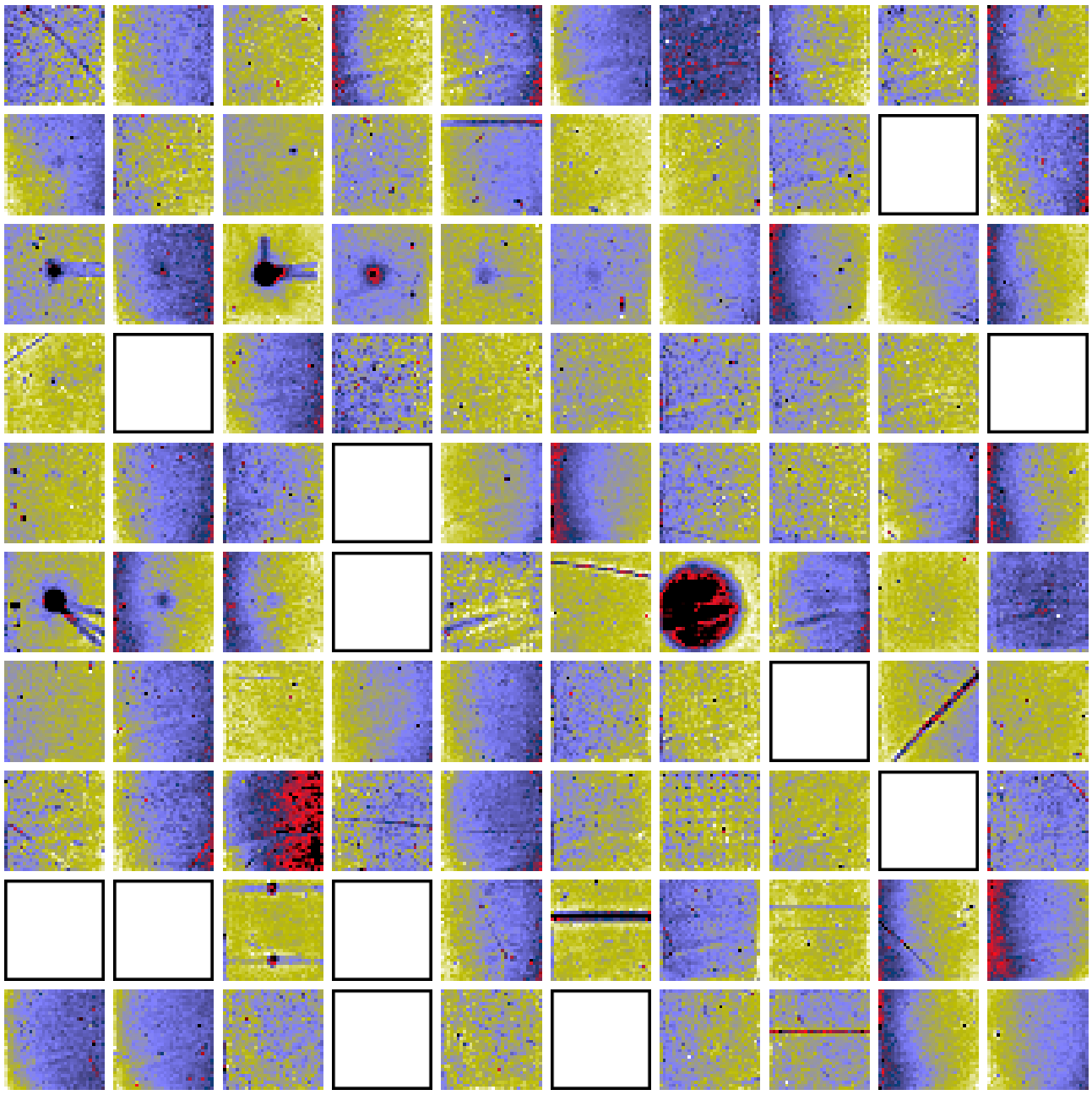

LW3 deactivation flat-field

Corrected for wheel jitter

Rev. 200 - 299

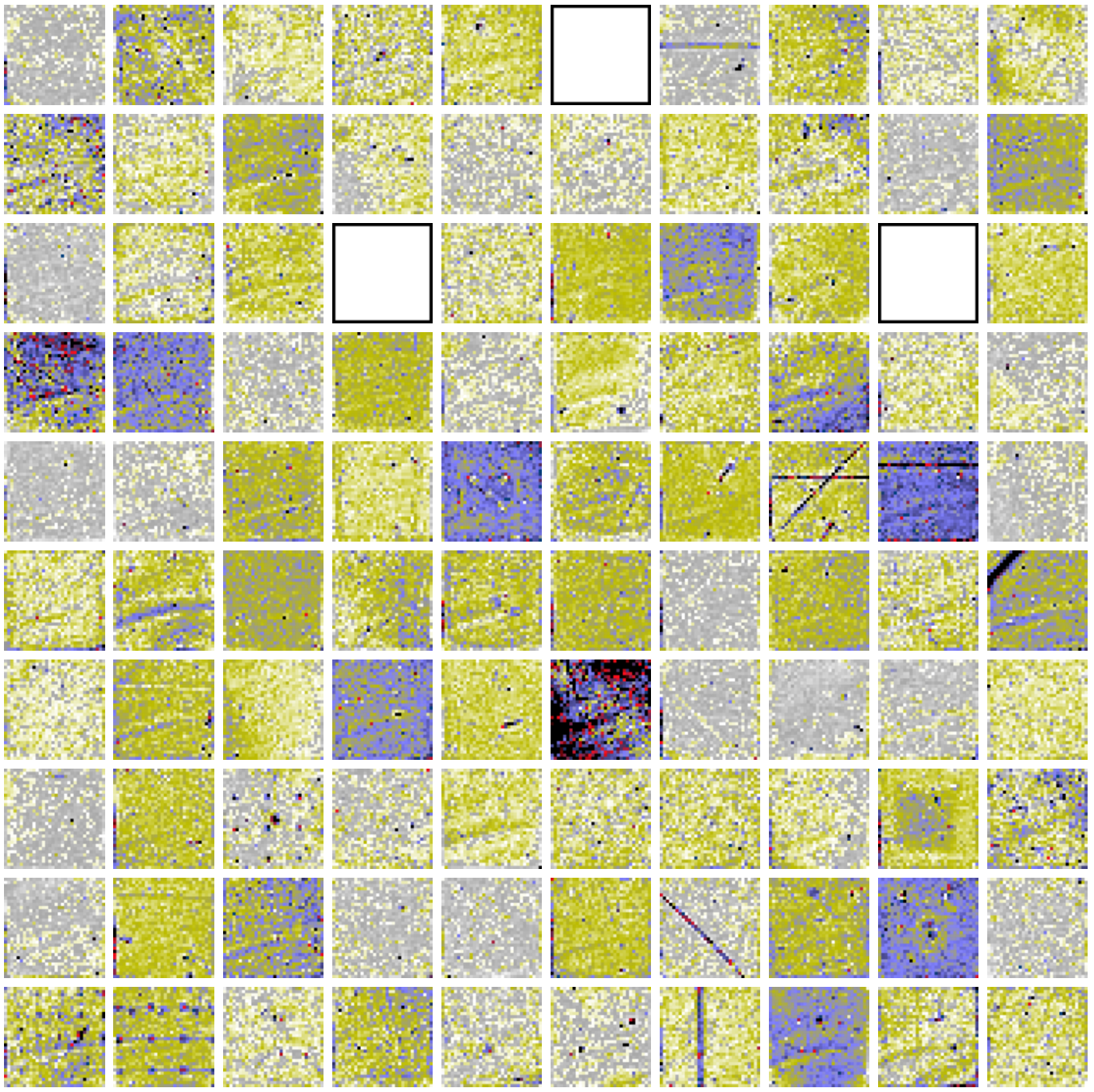

LW3 deactivation flat-field

Corrected for wheel jitter
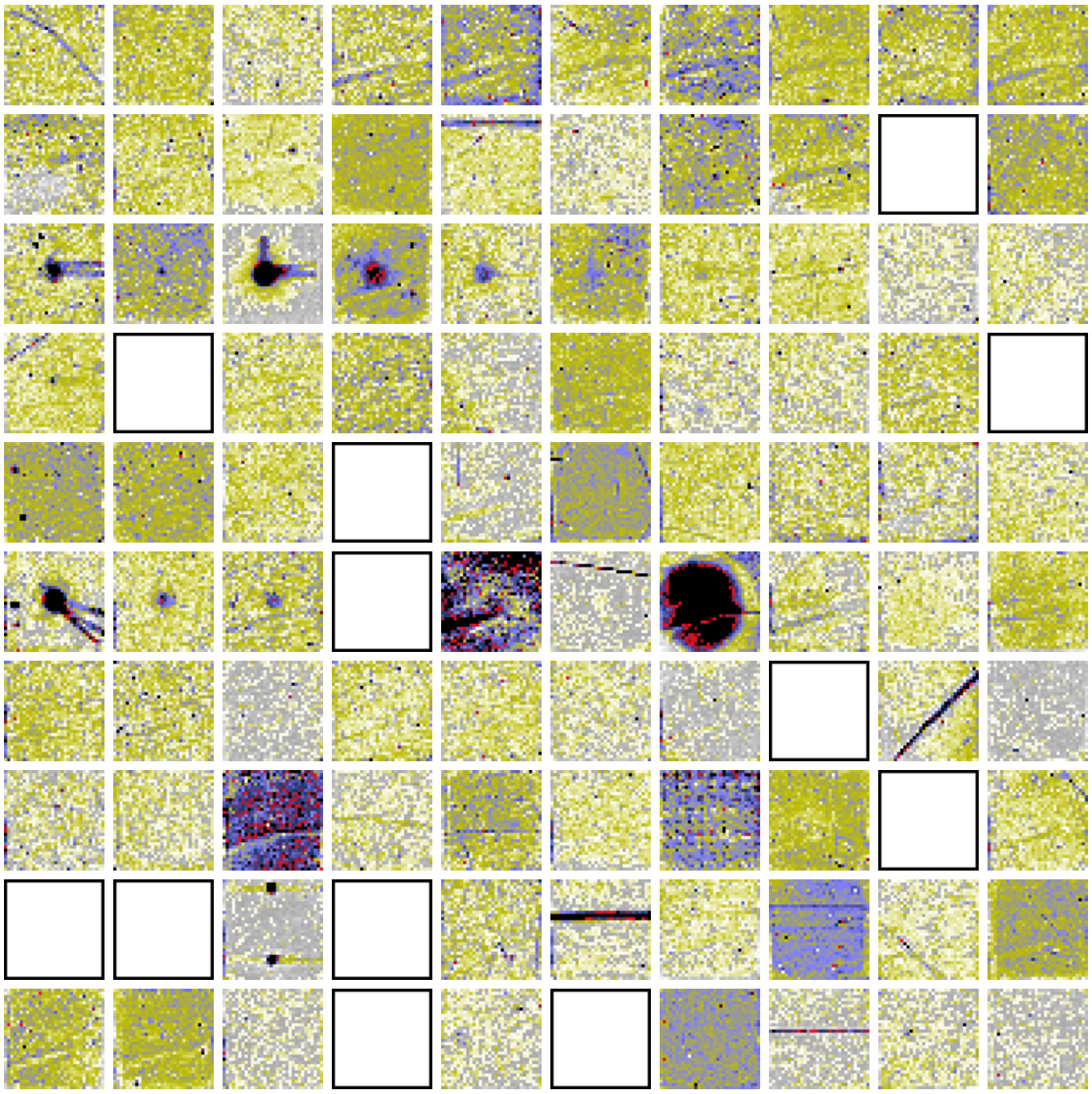
Rev. 500 - 599